JASA ARTICLE

Time reversal focusing in the audible range using a tunable sonic crystal

Valeria Sol Gomez,[a] Ignacio Spiousas,[b] and Manuel C. Eguia[c]
Laboratorio de Acústica y Percepción Sonora (LAPSo), Universidad Nacional de Quilmes, Consejo Nacional de Investigaciones Científicas y Técnicas (CONICET), Roque Saenz Peña 352, Bernal, Buenos Aires, B1876BXD, Argentina

ABSTRACT:
Time reversal (TR) focusing of acoustical waves is a widely studied phenomenon that usually requires a chaotic cavity or disordered scattering medium to achieve spatial and frequency decorrelation of the acoustic field when using a single channel. On the other hand, sonic crystals were disregarded as scattering media for the TR process because of their periodic structure and previous results showing poor spatial focusing when compared to a disordered medium. In this paper, an experimental realization of a tunable sonic crystal, which can achieve single-channel TR focusing amplitudes in the audible range comparable to those obtained in a disordered scattering medium, is presented. Furthermore, the tunable nature of the system allows it to switch the time-reversed pulse on and off by changing its geometrical configuration. A robustness analysis with respect to the perturbations in the sonic crystal configurations is also presented, showing that the time-reversed pulses with high temporal and spatial contrasts are preserved only for configurations that are close to the original one. © *2021 Acoustical Society of America.*
https://doi.org/10.1121/10.0005196
(Received 20 February 2021; revised 23 April 2021; accepted 16 May 2021; published online 11 June 2021)
[Editor: Yun Jing] Pages: 4024–4035

I. INTRODUCTION

Time reversal (TR) is a thoroughly studied signal processing technique (Cassereau and Fink, 1993; Derode *et al.*, 1995; Fink *et al.*, 2000) that allows wavefronts emitted from a source to focus back to the original emission point after some time. Since its original proposal by Fink and collaborators (Cassereau and Fink, 1993) more than three decades ago, TR has found a number of important applications in medicine (Fink *et al.*, 2003), nondestructive testing (Anderson *et al.*, 2017), underwater acoustics (Shimura *et al.*, 2013), and wireless communications (Montaldo *et al.*, 2004). In its simplest realization, the TR process consists of a first forward stage in which the impulse response (or short wideband pulse) from the source to an array of receivers is recorded and a second backward stage in which each recording is time-reversed and then reemitted from the receiver positions. As a result of the TR invariance, these backward waves converge in synchrony at the original source location (spatial focusing), and the initial pulse duration is recovered (temporal compression). The quality of this reconstruction increases with the aperture size of the array (termed TR mirror, TRM) and decreases with the spectral and spatial correlations of the wavefield (Derode *et al.*, 1998, 2001a,b).

In a seminal work, Derode *et al.* (1998) proposed and experimentally studied a TRM implementation using acoustic waves in a high-order multiple scattering medium (a disordered set of parallel steel rods in water). They showed not only that the pulse reconstruction was robust but also that compared to a homogeneous medium, it was also enhanced because of the greater effective aperture size and disorder-induced higher degree of decorrelation of the sound field.

Further works (Derode *et al.*, 2003; Derode *et al.*, 2000; Fink, 2006) showed that the quality of the temporal compression is mainly related to the spectral decorrelation, whereas the spatial focusing can be seen as an estimator of the correlation length (or the spatial correlation of the sound field). Thereby, the spatial resolution of the reconstructed peak does not depend on the opening of the array, therefore, a single receiver TR is feasible (single-channel focusing).

A schematic depiction of the TR process using one channel in a scatterer-filled medium is as follows. During the forward stage, the pulse is emitted from the source location A and scatters through the heterogeneities following different paths before reaching the receiver B. Therefore, the impulse response $h_{AB}(t)$ is formed by a superposition of pulses with arrival times corresponding to each of the acoustical paths followed by the scattering process. As the medium is disordered, the arrival times are uncorrelated and the impulse response is aperiodic. During the backward stage, the pulses are reemitted from B following the inverse sequence of arrival times in all directions $h_{AB}(-t)$. A portion of the wavefronts can trace back the forward paths and arrive in synchrony to the original location of the source A, creating a high amplitude pulse. However, there are other portions of the wavefronts which are emitted in directions different from those of the arrival, interfering at different times and locations and creating an incoherent background

[a]Also at: Comisión de Investigaciones Científicas de la Provincia de Buenos Aires (CIC), ORCID: 0000-0001-5944-072X.
[b]ORCID: 0000-0002-0283-4696.
[c]Electronic mail: meguia@unq.edu.ar, ORCID: 0000-0002-6515-8146.

https://doi.org/10.1121/10.0005196

signal. Two measures of the quality of the TR process can then be defined: the amplitude of the reconstructed pulse compared to the background signal at the source location for all times (temporal contrast) and the same amplitude compared to the background signal at the time of reconstruction for all other locations (spatial contrast). From a signal processing point of view, the reconstructed signal is the autocorrelation of the impulse response $h_{AB}(t)$ from the location of the source to the receiver, and the signal obtained at other locations C are the cross correlation between $h_{AB}(t)$ and the impulse response from B to C [$h_{BC}(t)$]. From this, it follows that the higher the temporal correlation of the impulse response (or by the Wiener-Kinchin theorem, the higher the spectral correlation), the lower the temporal contrast. If there are equivalent paths with the same time of arrival or periodicities creating correlations between the arrival times, these lead to the appearance of "sidelobes" in the autocorrelation function (Derode *et al.*, 2000). Also, if the spatial correlation of the medium is higher, this can be reflected in a higher cross correlation between $h_{AB}(t)$ and $h_{BC}(t)$ and, therefore, the spatial contrast is lowered. In this way, both the spatial decorrelation and temporal (or spectral) decorrelation, such as those created by a heterogeneous medium, are required to reconstruct the original pulse through the TR process. Furthermore, Tourin *et al.* (2006) have found that when the medium is less heterogeneous, for example, using a phononic crystal instead of a random array of scatterers, the spatial focalization phenomenon is lost. Indeed, the discrete translational symmetries of the medium introduce spatial correlations in the scattered field and lead to a reduction of the spatial focusing. Surprisingly, the temporal contrast was better for the case of the phononic crystal compared to a disordered medium for frequencies within the stopping band. The authors concluded that disorder is a key point to achieve TR. Perhaps because of this lack of spatial focusing that was reported by Tourin *et al.* (2006), no further experimental work was conducted using TR and phononic (or sonic) crystals despite the many interesting properties that are exhibited by these periodic composite materials (Cervera *et al.*, 2001; Lu *et al.*, 2007; Sanchez-Perez *et al.*, 1998). On the other hand, Lemoult *et al.* (2011) studied TR using another periodic structure, an array of acoustic resonators, and showed that subwavelength focusing using TR is also possible in this medium. Further works showed the advantage of using periodic arrays of resonators for subwavelength focusing and nearly "perfect" TR, sinking the energy of the refocused peak (Kaina *et al.*, 2015; Lemoult *et al.*, 2013; Ma *et al.*, 2020; Ma *et al.*, 2018).

In this work, we revisit the TR technique using a sonic crystal in the audible range, taking advantage of another feature of this periodic composite material: the ability to tune its transmission properties by changing its geometric configuration. We will show that, despite the spatial correlations induced by the periodicities of the system, it is possible to reproduce the original experiment of Derode *et al.* (2003), yet, with precise control of the scattering medium. Previous studies (Blomgren *et al.*, 2002; Derode *et al.*, 2000, 2001b; Papanicolaou *et al.*, 2004) have proved that TR focusing is a statistically stable phenomenon, i.e., it does not depend on a particular realization of the heterogeneous medium. However, when the medium changes in between the forward and backward stages of the TR, the focusing is destroyed for changes that are larger than the average wavelength (Vigo *et al.*, 2004). Therefore, we expect that we may be able to switch on and off the TR pulse by changing the geometric configuration of the crystal.

This paper is organized as follows. Section II is devoted to the description of the experimental setup and also introduces the methods and definitions to be employed for the rest of the paper. In Sec. III, we present the study of the temporal and spatial contrasts of the time-reversed focusing. An analysis of the robustness of the system is presented in Sec. IV. Finally, in Sec. V, we discuss our results as they relate to previous works, and in Sec. VI, we summarize our findings.

II. MATERIALS AND METHODS

A. Sonic crystal

For the recordings, we used a variable-geometry sonic crystal structure made up of 100 squared U-shaped wooden columns with sides of 0.15 m and 2.70 m of height. The columns are distributed in a square lattice arrangement with a spatial periodicity of 0.3 m. Each column can rotate independently around the vertical axis using a stepper motor and reduction system to overcome inertia effects. We defined a sonic crystal configuration as a state determined by the angular position of all of its columns. The configuration C0, displayed in Fig. 1(a), has all of the U-shaped faces toward the front of the structure, an orientation that will be considered $angle = 0$, from which each column can rotate 135° in both directions. As a reference, in Fig. 1(c), we display the band structure diagram for the sonic crystal in the C0 configuration. The lines correspond to combinations of frequencies and wave vectors ($\boldsymbol{k}$) following the contour of the irreducible Brillouin zone and were calculated as the eigenvalues of the primitive cell with periodic boundary conditions using the finite element method.

B. Room

The measurements were performed in a rectangular room with a floor that is 12×7 m with a height of 3 m. The room was covered with absorbent panels of pyramid acoustical foam (50 mm), carpet on the floor, and acoustic fiberglass panels on the ceiling. With this configuration, the room had full- and limited-band reverberation times of 0.45 s and 0.14 s, respectively (for 0.02–20 kHz and 0.5–20 kHz, respectively).

C. Hardware

The sound source (Genelec 8030B loudspeaker, Genelec, Finland) was located 0.77 m behind the sonic crystal structure and centered in the longitudinal direction at 1.62 m high. The receiver (Sennheiser Ambeo VR microphone, Sennheiser, Germany) was also located at a height of

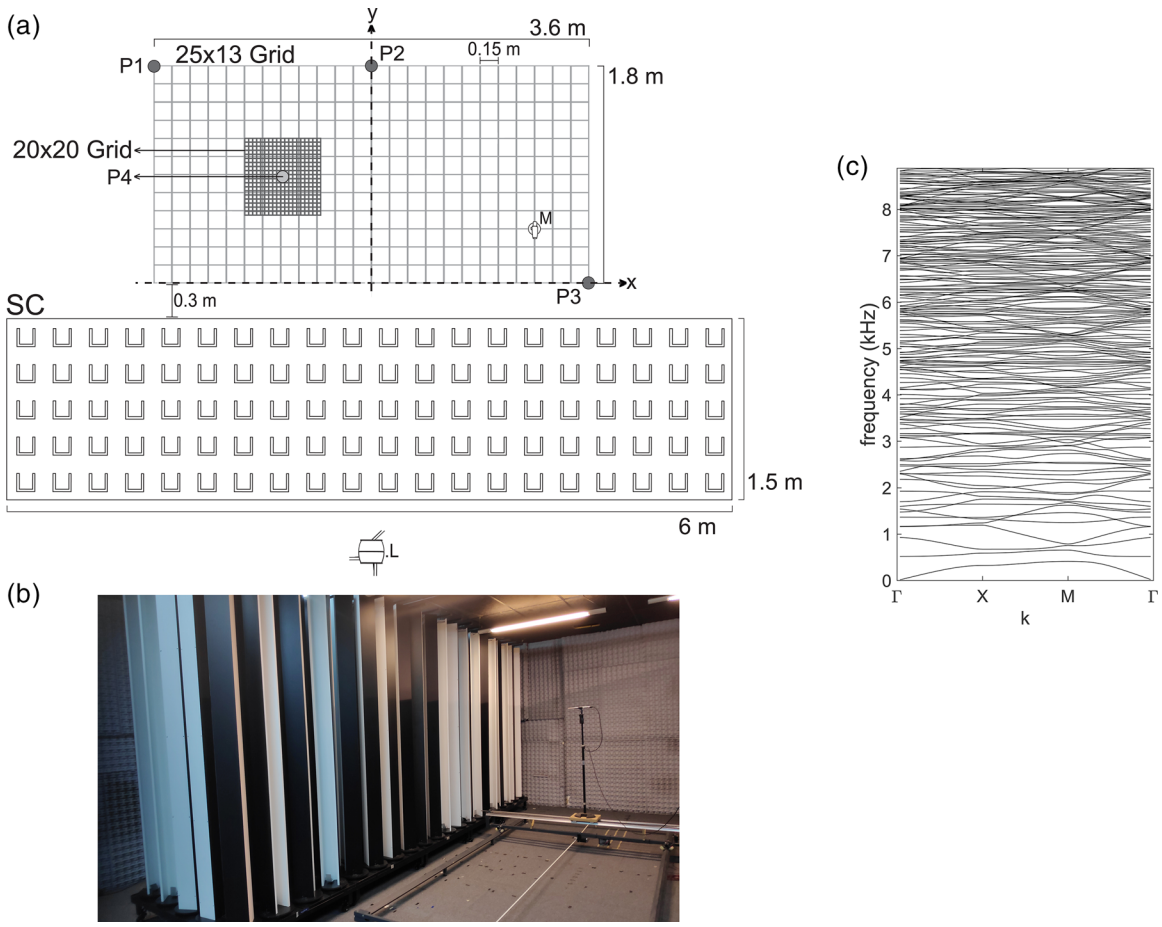

FIG. 1. (Color online) The experimental setup. (a) The schematic representation of the sonic crystal, loudspeaker (L), measuring grids, and coordinate system as seen from above. The 100 U-shaped columns of the sonic crystal are oriented toward the front of the structure (C0 configuration). The measuring grid is 3.6 m wide × 1.8 m long and has a recording point every 0.15 m in both axes. The recordings in points P1–P3 were used for the spatial and temporal contrast robustness analysis. The recordings in point P4 and the narrow grid around it were used for the calculation of the reduced spatial contrast (see Sec. II G). (b) The picture of the device mounted in the room where the recordings took place. On the right, the motorized recording system (described in Sec. II C) can also be seen. (c) The band diagram of the sonic crystal in the C0 configuration showing the eigenfrequency dependence on the wave vector along the standard $\Gamma XM\Gamma$ path.

1.62 m. The source and receiver were controlled by a MOTU mk3 hybrid sound card (MOTU, USA) and a Mac Mini computer (USA). All of the sound samples were recorded with a sample frequency of 96 kHz. For the recordings, we moved the microphone using a custom-made automated trolley that allowed us to change the position of the microphone on two axes with millimeter resolution in a maximum area of 4.16 m × 2 m.

D. Impulse response recordings

Impulse responses were obtained using the logarithmic sweep method (Farina, 2000) with a sweep covering the frequency range between 0.5 and 20 kHz over a period of 20 s. The lower limit of the frequency range was set to 0.5 kHz to avoid both the relative higher reverberation time of the room below this frequency (see Sec. II B) and the first full bandgap [see Fig. 1(c)]. These impulse response measurements were obtained throughout the field of study, delimited by the dimensions of the automatic trolley using a 3.6 × 1.8 m 25 × 13-point square grid with each point separated by 0.15 m [see Fig. 1(a)].

A complete grid of the impulse responses was recorded for different sonic crystal configurations. For this study, we used two disordered configurations, which we call R1 and R2, determined by 2 sets of 100 angles chosen randomly from a uniform distribution between −135 and 135 deg, and an ordered configuration, the C0 configuration defined above. We also recorded the full grid in the empty room for the sake of comparison.

E. Temporally reversed pulse

The recorded sweep is processed (according to Farina, 2000) to obtain the impulse response at the corresponding measurement point. Then, the impulse response is temporarily reversed, played back, and recorded at that same measurement point. Therefore, we can obtain the recording of a time-reversed pulse at each point of the grid for a given configuration of the sonic crystal.

For the rest of the paper, we will use the notation $h(t)^{c_k}_{\boldsymbol{x}_i}$ for the impulse response recorded at the point $\boldsymbol{x}_i$ with the sonic crystal set with the c_k configuration.

https://doi.org/10.1121/10.0005196

F. Formulas and definitions

The cross correlation of two impulse responses, one recorded with the configuration c_k and measured at the point $\boldsymbol{x}_i$ and the other one recorded with the configuration c_l and recorded at the point $\boldsymbol{x}_j$, is defined by

$$X\text{corr}^{c_k\to c_l}(t;\boldsymbol{x}_i,\boldsymbol{x}_j)=\int_{-\infty}^{\infty} h(\tau)_{\boldsymbol{x}_i}^{c_k} h(\tau+t)_{\boldsymbol{x}_j}^{c_l} d\tau. \tag{1}$$

This function, using the equivalence of this cross correlation operation with the convolution after reversing the second function in time, can be rewritten as

$$X\text{corr}^{c_k\to c_l}(t;\boldsymbol{x}_i,\boldsymbol{x}_j)=h(t)_{\boldsymbol{x}_i}^{c_k} * h(-t)_{\boldsymbol{x}_j}^{c_l}, \tag{2}$$

which, in turn, is equivalent to the signal obtained using the TR process given that the forward stage is recorded with configuration c_k and the backward stage is recorded with configuration c_l. It is worth noticing that Xcorr becomes the autocorrelation function when $c_k = c_l$ and $\boldsymbol{x}_i = \boldsymbol{x}_j$. This function has its maximum value for the time of reversal $t = 0$, which when $h(t)$ is finite, discrete, and has length L corresponds to the sample $L + 1$ of the autocorrelation of the signal.

For the following calculations, to compare recordings with different pressure levels, we will use a normalized version of the correlation function by simply dividing $X\text{corr}^{c_k\to c_l}(t;\boldsymbol{x}_i,\boldsymbol{x}_j)$ by its value at the time of reversal $t = 0$ and for $\boldsymbol{x}_j = \boldsymbol{x}_j$,

$$\tilde{X}\text{corr}^{c_k\to c_l}(t;\boldsymbol{x}_i,\boldsymbol{x}_j)=\frac{X\text{corr}^{c_k\to c_l}(t;\boldsymbol{x}_i,\boldsymbol{x}_j)}{X\text{corr}^{c_l\to c_l}(t=0;\boldsymbol{x}_j,\boldsymbol{x}_j)}. \tag{3}$$

1. Temporal contrast

The temporal contrast is a measure of how concentrated (or compressed) in time the time-reversed signal is. It is calculated by measuring the energy ratio between the peak at the time of reversal $t = 0$ and the rest of the signal in the temporal domain (Hudin *et al.*, 2014). We will use two alternative measures of the temporal contrast, each is better suited to describe a particular characteristic of the temporal reversion, the root mean square (RMS) temporal contrast (TC_{RMS}) and the peak temporal contrast (TC_{peak}; Alberti *et al.*, 2019).

We first define the RMS of a function $f(t)$ over an arbitrary interval (not necessarily connected) T_{int} as

$$\text{RMS}[f(t\in T_{\text{int}})]=\sqrt{\frac{\int_{t\in T_{\text{int}}} f(t)^2 dt}{\int_{t\in T_{\text{int}}} dt}}. \tag{4}$$

We then apply this RMS measure to the cross correlation function over a portion of the signal adjacent to the time of reversal ($t = 0$), excluding the peak, and compare it with the value at the time of reversal to define our first measure of the temporal contrast TC_{RMS},

$$\text{TC}_{\text{RMS}}^{c_k\to c_l}(\boldsymbol{x}_i)=\frac{\tilde{X}\text{corr}^{c_k\to c_l}(t=0;\boldsymbol{x}_i,\boldsymbol{x}_i)}{\text{RMS}\left[\tilde{X}\text{corr}^{c_k\to c_l}(t\in T_{\text{int}};\boldsymbol{x}_i,\boldsymbol{x}_i)\right]}, \tag{5}$$

where T_{int} is an interval around the time of reversal, excluding the potential time-reversed peak, and it is defined as

$$T_{\text{int}}=\left(-\frac{\Delta_t}{2}<t<-\frac{w_t}{2}\right)\cup\left(\frac{w_t}{2}<t<\frac{\Delta_t}{2}\right), \tag{6}$$

where Δ_t is the width of the user-defined time interval (100 ms in our case) and w_t is a typical width of the peak (0.5 ms in our case). This last interval is added to minimize the influence of the peak and background noise on the RMS calculation.

This definition of temporal contrast (TC_{RMS}) gives us information on how the energy is concentrated in the peak region despite how it is spread in that region (e.g., if the signal is "smooth" or presents "secondary" peaks).

To account for the possible appearance of secondary peaks in the amplitude, as it could happen in a system with spatial symmetries, a second definition of the temporal contrast compares the amplitude of the peak with the amplitude of the second peak of the $\tilde{X}$corr function (Alberti *et al.*, 2019). We define it as the peak temporal contrast (TC_{peak})

$$\text{TC}_{\text{peak}}^{c_k\to c_l}(\boldsymbol{x}_i)=\frac{\tilde{X}\text{corr}^{c_k\to c_l}(t=0;\boldsymbol{x}_i,\boldsymbol{x}_i)}{\max\left[\tilde{X}\text{corr}^{c_k\to c_l}(t\in T_{\text{int}};\boldsymbol{x}_i,\boldsymbol{x}_i)\right]}. \tag{7}$$

In this case (TC_{peak}), the temporal contrast is sensitive to secondary peaks in the amplitude and not to the total energy of the "non-peak" region (T_{int}).

2. Spatial contrast

The spatial contrast quantifies the energy ratio between the peak of the $\tilde{X}$corr function at the temporal reversion point and the same function calculated on any other point of the space (the measuring grid in our case).

As with the temporal contrast, we will define two versions of the spatial contrast: SC_{RMS} and SC_{peak},

$$\text{SC}_{\text{RMS}}^{c_k\to c_l}(\boldsymbol{x}_i)=\frac{\tilde{X}\text{corr}^{c_k\to c_l}(t=0;\boldsymbol{x}_i,\boldsymbol{x}_i)}{\text{RMS}\left[\tilde{X}\text{corr}^{c_k\to c_l}(t=0;\boldsymbol{x}_i,\boldsymbol{x}\neq\boldsymbol{x}_i)\right]}, \tag{8}$$

and

$$\text{SC}_{\text{peak}}^{c_k\to c_l}(\boldsymbol{x}_i)=\frac{\tilde{X}\text{corr}^{c_k\to c_l}(t=0;\boldsymbol{x}_i,\boldsymbol{x}_i)}{\max\left[\tilde{X}\text{corr}^{c_k\to c_l}(t=0;\boldsymbol{x}_i,\boldsymbol{x}\neq\boldsymbol{x}_i)\right]}. \tag{9}$$

It worth noticing that because the samples were recorded in a discrete grid, for all of the calculations in this paper, $\boldsymbol{x}\neq\boldsymbol{x}_i$, will actually by discretized as $\boldsymbol{x}_j$ with $j\neq i$.

Both the temporal and spatial contrasts are scalar magnitudes, which are calculated for a given pair of sonic crystal configurations (c_k and c_l) and a specific point in the spatial domain (x_i). These magnitudes will be expressed in nondimensional units.

3. Propagation matrix and time-reversal operator

To further analyze the spatial and spectral correlations of the acoustic field, we will also make use of the propagation matrix and TR operator as a function of the frequency and space as defined in Derode *et al.* (2003).

The propagation matrix $H_j(\omega)$ is the Fourier transform of the point to point impulse response between the source and measurement point $\boldsymbol{x}_j$. In our case, this corresponds to a $1 \times M$ (1×325) row vector because we are using a single source and $M = 325$ measurement points (the grid of 13 $\times$ 25 points is row ordered). The time-reversal transfer function between the measurement points $\boldsymbol{x}_i$ and $\boldsymbol{x}_j$, $\mathrm{TRTF}_{ij}(\omega)$, is defined as the outer product of the propagation matrices of the corresponding points and is computed for a fixed configuration c_k as

$$h(t)_{\boldsymbol{x}_i}^{c_k} \rightarrow H_i^{c_k}(\omega), \tag{10}$$

$$\mathrm{TRTF}_{ij}^{c_k}(\omega) = \left[H_i^{c_k}(\omega)\right]^{*T} H_j^{c_k}(\omega). \tag{11}$$

Then TRTF is an $M \times M$ matrix, depending on the frequency, where the ith row corresponds to the frequency response of the whole set of measurement points when the impulse response of the $\boldsymbol{x}_i$ measurement point is chosen for the TR operation. After integrating this transfer function over the frequency, we obtain the TR operator,

$$\mathrm{TR}_{ij}^{c_k} = \int \mathrm{TRTF}_{ij}^{c_k}(\omega) d\omega, \tag{12}$$

$$\mathrm{TR}_{ij}^{c_k} = \tilde{X}\mathrm{corr}^{c_k \rightarrow c_k}(t = 0; \boldsymbol{x}_i, \boldsymbol{x}_j). \tag{13}$$

For a discrete signal, this last expression corresponds to a summation over the frequency indices or the inner product along the frequency axis. This matrix has two possible interpretations, which will be discussed later. The first is more direct and relates each TR_{ij} element to the spectral cross correlation of the transfer functions of the points $\boldsymbol{x}_i$ and $\boldsymbol{x}_j$. The second interpretation arises from the fact that the integral in Eq. (12) is also the inverse Fourier transform of the TR transfer function evaluated at the time of reversal ($t = 0$). Hence, the ith row of TR is equivalent to the amplitude value of the acoustic field of the M measurement points at the time of reversal.

G. Sonic crystal configurations and robustness analysis

What we call a sonic crystal configuration (the angular position of the n scatterers) can be represented as a point in an n-dimensional space. With this in mind, we defined the distance between the configuration as the Euclidean norm of the difference between the position in this n-dimensional space in degrees. In our case, $n = 100$ and each scatterer angle ranges from -135 to 135 deg.

To study how the TR effect reacts when the sonic crystal configuration is modified, we will propose three different kinds of perturbations on the 100-dimensional space: (1) displacement on a straight line between two given configurations, (2) perturbations along a random line starting from a given configuration, and (3) small perturbations on a single coordinate (orthogonal displacements) from a given configuration.

For the type (1) perturbation, we moved on a straight line from R1 to R2 configurations on 20 equidistant steps. To do so, we shifted each scatterer by 1/20 of the angular distance for R1 and R2. This is equivalent to moving from R1 to R2 in the 100-dimensional space on a straight line and with equidistant steps in distance. To determine how likely it is to obtain two random configurations that differed by each of such steps, we simulated 10 000 random configurations generated by randomly assigning a scatterer angle between -135 and 135 deg with equal probability (i.e., angles drawn from a uniform distribution). Then, we calculated the Euclidean distance between each configuration and the other ones and estimated the probability density function of observing a given distance (Fig. 2). In Fig. 2, we can see that the distances between random configurations smaller than the 15 first steps from R1 to R2 are extremely rare to find by mere chance ($p < 3.4E - 4$).

For this first type of perturbation, we measured the time-reversed response in three points (P1–P3 in Fig. 1). We first recorded the forward phase on each measuring point and normalized it with the autocorrelation. Then, we shifted the position of the scatterers by 1/20 on the R1-R2 direction, played the inverted response, and recorded it in each measuring point. We repeated this procedure for each of the 20 perturbation steps.

The type (2) perturbations are implemented by starting from a random configuration and moving in a given direction in the 100-dimensional space. We repeated this perturbation for nine given distances, which can be interpreted as radii of 100-dimensional concentric spheres in the configuration space, and five random directions for each distance.

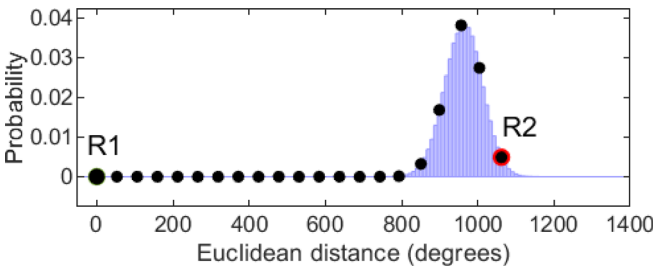

FIG. 2. (Color online) The distribution of Euclidean distances of randomly generated sonic crystal configuration. The histogram represents the probability function distribution of the Euclidean distance calculated using the distances of 10 000 simulated sonic crystal configurations with each other. The black dots represent the 20 Euclidean-distance steps from R1 (green dot) to R2 (red dot) used for the type (1) robustness analysis.

https://doi.org/10.1121/10.0005196

We moved from each of the ten initial random configurations to a distance of 200 deg in nine quasi-logarithmic steps (distances equal to 5, 10, 20, 35, 50, 75, 100, 150, and 200 deg). The forward phase was recorded for each of the initial random configurations (0 deg distance) in points P1–P3. Then, after time inversion and normalization using the autocorrelation, the backward phase was recorded in each point and for each distance and direction (radius and angle). We averaged the temporal contrast across directions for each radius and studied its relationship with distance.

To explore the variations in the spatial contrast, we repeated the procedure for point P4 and the reduced grid [Fig. 1(a)] around it. In this case, we calculated the forward phase on P4 for each random initial configuration and backward phase for each distance and direction in P4 and all the points in the reduced grid. We then calculated one value of the spatial contrast for each distance and direction and averaged across the directions, obtaining a value of (reduced) spatial contrast for each distance.

The goal of this perturbation was to generalize the results obtained with type (1) by exploring random initial configurations and random perturbation directions in a very small neighbourhood of R1 in the configuration space (up to a Euclidean distance of 200 deg).

Finally, type (3) perturbations consist of moving each scatterer one at a time by a given angle (± 15 deg) starting from R1. The direction of the shift was randomly assigned unless it was not possible to move 15 deg in one direction. Here, we want to study how a movement in a given coordinate (angle of a scatterer) affects the TR. In this last perturbation, the configuration shifts in the distance space only on orthogonal movements starting from R1.

III. TR FOCUSING

In this section, we will show that the TR focusing phenomenon is feasible using our variable-geometry sonic crystal with *U*-shaped scatterers and the focused peak can be switched on and off by changing the geometric configuration of the crystal.

Using the method described in Sec. II D, we obtained a recording of the refocused peak for the measurement points (see Fig. 1) that showed no significant differences when comparing it to the autocorrelation function of the impulse response (see comparison in supplementary Fig. S1).[1] Thus, in the following, we can confidently make use of the cross correlation function and Eqs. (5)–(9) for computing the temporal and spatial contrasts of the refocused peak for all of the 25×13 points in the measurement grid. All of the following acoustical magnitudes were calculated using the *W* channel of the Ambisonics *B*-format recording (the *X*, *Y*, and *Z* channels can be found, for the sake of completeness, in the supplementary Figs. S2, S3, and S4, respectively[1]).

To highlight the switching behavior of the TR focusing, we will compare two scenarios: first, an ordinary TR process in which the same sonic crystal configuration (R1) is used during the forward (impulse response recording) and backward (reversed impulse response emission) phases ($R1 \rightarrow R1$), and a second scenario in which we change the configuration to R2 during the backward phase ($R1 \rightarrow R2$). The temporal and spatial contrasts for both scenarios, computed using Eqs. (5)–(9) for all of the grid points, are compared in the left and right columns of Fig. 3.

The values of the temporal contrast obtained for the $R1 \rightarrow R1$ scenario at the measurement grid points ranged between 35 and 70 for TC_{RMS} and between 5 and 15 for TC_{peak}. The spatial contrast ranged between 15 and 40 for SC_{RMS} and between 3 and 15 for SC_{peak}. The TC_{RMS} and SC_{RMS} values obtained are within the range that previous studies reported when using scattering with ultrasound and audible sound focusing in rooms (Ribay *et al.*, 2005; Yon *et al.*, 2003).

Moreover, the contrast measures obtained when the sonic crystal configuration is changed during the backward phase ($R1 \rightarrow R2$) are dramatically reduced, showing the sensitivity of the system to changes in the propagation medium. This difference is less evident for measurement points close to the $x = 0$ axis due to two different factors.

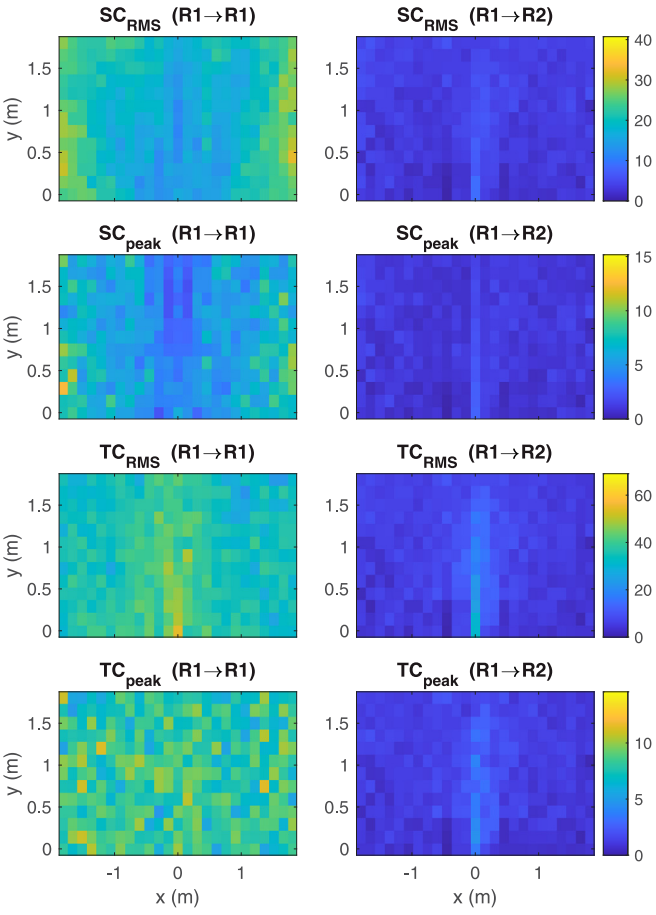

FIG. 3. (Color online) The temporal and spatial contrasts. The plots in the left column show the magnitudes calculated with the forward and backward phases corresponding to the R1 configuration ($R1 \rightarrow R1$), whereas for plots in the right column, the backward phase was obtained using R2 ($R1 \rightarrow R2$). The first two rows show the spatial contrasts (SC_{RMS}, SC_{peak}), and the last two rows show the temporal contrasts (TC_{RMS}, TC_{peak}) calculated following Sec. II F. The *x* and *y* axes represent the locations of the recording point in the measuring grid as defined in Fig. 1(a).

First, $x=0$ is a symmetry axis of the experimental setup, including the sonic crystal grid. Even if this symmetry is broken by the random orientation of the columns, a spatial correlation for the lower frequencies persists as we will show in Sec. V. This correlation is higher for the measurement points that are closer to the symmetry axis. As a consequence, the spatial contrasts (particularly SC_{peak}) decrease as we approach the $x=0$ axis. The second factor is the prominence of the ballistic part of the impulse response (Derode *et al.*, 2001a) for the measurement points situated over $x=0$. In fact, from this line, it is possible to have visual contact with the loudspeaker in between the columns. This ballistic part contributes equally to the amplitude of the acoustic field at the reversal time for both configurations. Therefore, the contrast measures are still significant at $x=0$ for the $R1 \rightarrow R2$ scenario.

To check if the refocused peak was caused by the sonic crystal and that it was not a mere effect of the room, we also computed the cross correlation $\tilde{X}\mathrm{corr}(t;\boldsymbol{x}_i,\boldsymbol{x}_j)$ for the impulse responses measured in the room without the sonic crystal. The amplitude of the cross correlation at the time of reversal $t=0$ for all measuring points $\boldsymbol{x}_j$ is displayed in supplementary Fig. S5, using four examples of recording points $\boldsymbol{x}_i$.[1] In all cases, we observed a wavefront corresponding to the direct sound and no refocusing peaks. We also computed the spatial and temporal contrast without the sonic crystal (see supplementary Fig. S6[1]).

The possibility of switching the TR focusing on and off by changing the sonic crystal configuration during the backward phase is further illustrated in Fig. 4. The normalized cross correlation function, defined by Eq. (3), is computed at the time of reversal for all measurement points and the two scenarios $R1 \rightarrow R1$ (left panels) and $R1 \rightarrow R2$ (right panels), taking five recording points (rows) as examples. As we previously mentioned, this is equivalent (normalization apart) to the acoustic field obtained under the two scenarios at the reversal time (time-reversed acoustic field). The first three rows display neat time-reversed peaks, which are completely lost when the configuration is changed during the backward phase. It is worth noticing that this effect is present even for the farthest recording point (first row). In the last two rows, we display two examples where the switching effect is not completely achieved. Even when the time-reversed peak is still high, there are residual peaks after switching the sonic crystal configuration to R2, and a "phantom" peak in the symmetric (relative to the $x=0$ axis) measurement points. This also can be explained by the previously mentioned ballistic wavefront and spatial correlation factors. An animated figure displaying the time-reversed acoustic field for both configurations and all points is provided in Mm. 1.

Mm. 1. Animation of the time-reversed acoustic field for both configurations and all points. This is a file of type "gif" (48360 KB).

Thus far, we have only used configurations R1 and R2 as representatives of two different random configurations

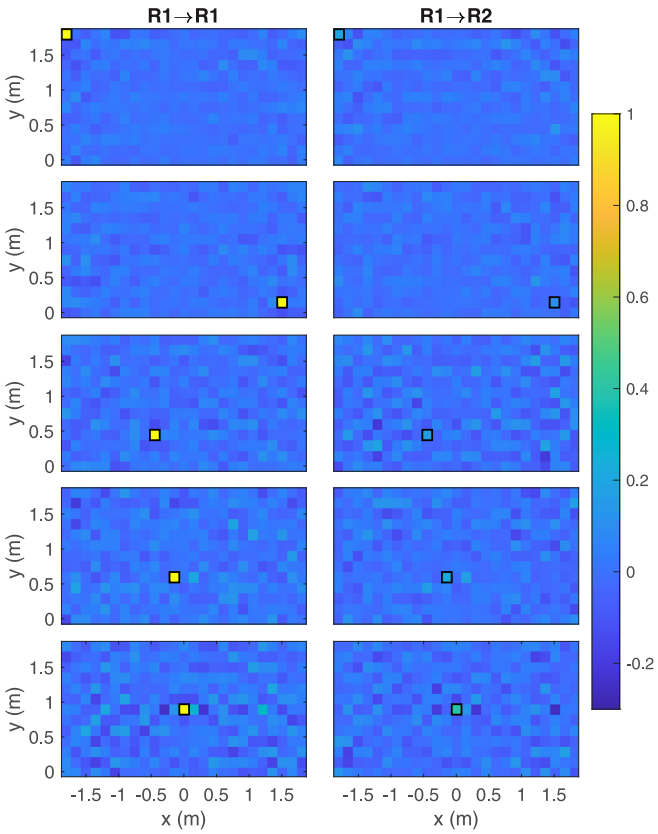

FIG. 4. (Color online) The amplitude of the normalized cross correlation function given by Eq. (3) at the time of reversal $t=0$ for all measuring points $\boldsymbol{x}_j$, using $R1 \rightarrow R1$ (left column) and $R1 \rightarrow R2$ (right column), and five examples of the forward recording points $\boldsymbol{x}_i$ (as rows). The positions of the forward recording points are indicated by the hollow black squares. The brighter squares represent better time reversions, and the x and y axes represent the location of the measuring point $\boldsymbol{x}_j$ in the grid, as defined in Fig. 1(a). The amplitudes are represented in normalized units (see Sec. II F).

because their distances in configuration space fall within a typical range (see Fig. 2). However, one may now ask how this difference in contrast changes as the distance between the configurations is reduced. Also, we are interested in studying how well the high values of contrasts are preserved for small variations in the geometric configuration between the forward and backward phases. To address these two questions, we will perform a robustness analysis for the contrast magnitudes within the configuration space.

IV. ROBUSTNESS ANALYSIS

In this section, we will analyze how robust the TR focusing phenomenon is regarding changes in the sonic crystal configuration (i.e., its geometry). We will make use of the configuration space defined in Sec. II G and take the three different approaches described therein.

In Fig. 5, we display the temporal contrasts for a measured time-reversed focusing peak in three points (P1–P3 in Fig. 1) using the impulse response obtained in the forward phase with the configuration R1 as the configuration for the backward phase is switched from R1 to R2 in discrete steps. This magnitude is expressed as the Euclidean distance

https://doi.org/10.1121/10.0005196

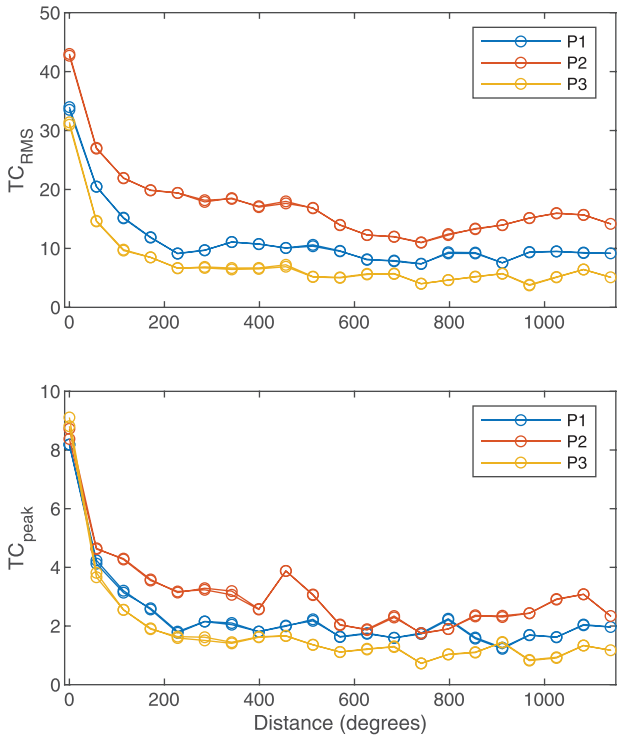

FIG. 5. (Color online) The temporal contrast as a function of the distance between the R1 and R2 sonic crystal configurations. The temporal contrast is obtained by recording the forward phase with the R1 configuration and the backward phase for a shifted configuration. The backward configuration was varied from R1 to R2 in 20 equal discrete steps (x axis, as defined in Sec. II G). The configuration was shifted in a forward (R1 to R2) and backward (R2 to R1) direction, resulting in two recordings for all of the intermediate configurations (overlapped in the plot). The signals were recorded in points P1–P3 and contrasts are given in nondimensional units.

(defined in Sec. II G) relative to R1 in the configuration space. The intermediate points in Fig. 5 correspond to the black dots in Fig. 4. Both contrast measures decrease rapidly with distance. For distances below 200 (configurations similar to R1), we still have a residual contrast. Nevertheless, the probability of obtaining such a similar configuration (distance < 200) by mere chance is less than 10^{-54} (based on the simulated distance distribution in Sec. II G).

In Fig. 6 (left panels), we display the temporal contrast measures as a function of the distance in the configuration space using the type (2) perturbation analysis method described in Sec. II G for the same three points P1–P3. These contrasts are normalized to the maximum contrast obtained for the R1 configuration. This study can be seen as a "zoom in" into the decaying part of the curves displayed in Fig. 5. The dots correspond to the different starting points and perturbation directions for a fixed radius of the hypersphere, and the lines correspond to their mean values averaged over all directions and starting points in the configuration space. In this perturbation study, we also analyzed the spatial contrast values as a function of the distance. This is displayed in the right column of Fig. 6. In both cases, a gradual decay of the contrast values is observed up to a distance of 200 deg.

The relative variation of TC_{RMS} with respect to the perturbations of the individual scatterers [the type (3) perturbation method described in Sec. II G] for the same measurement points (P1–P3) is shown in the three respective panels of Fig. 7. We define the relative contrast perturbation magnitude as $1 - TC^{pert}_{rms}/TC_{rms}$, where TC^{pert}_{rms} (TC_{RMS}) is the RMS temporal contrast measure of the perturbed (unperturbed) configuration. In all cases, the contrast values obtained with the perturbed configurations were

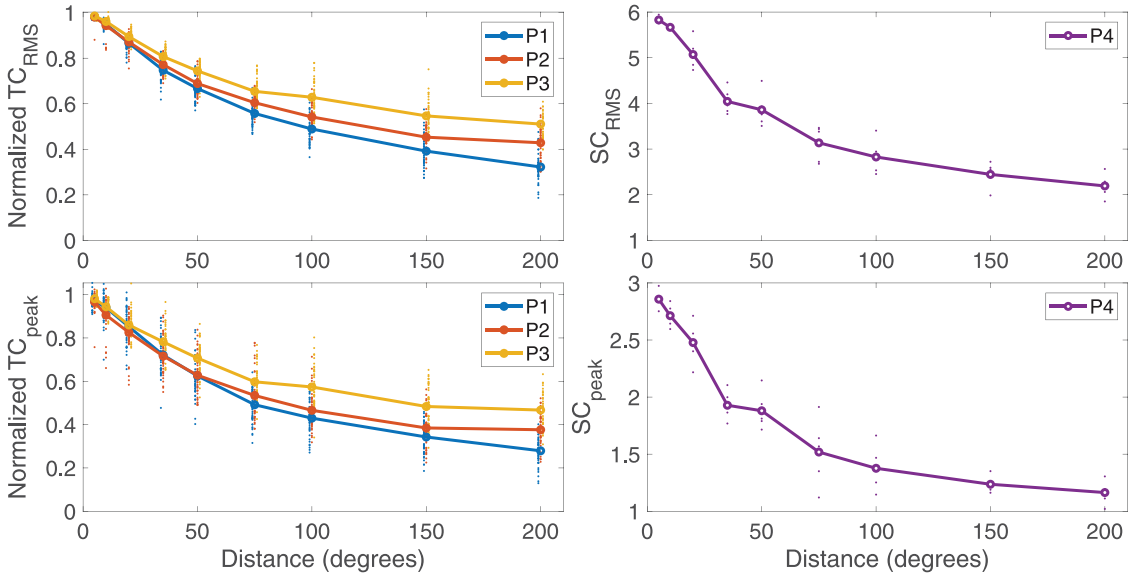

FIG. 6. (Color online) The temporal and spatial contrasts as a function of the distance for sonic crystal configurations used in the backward phase in a small neighbourhood of the configuration (R1) used in the forward phase. In the left column, we show the temporal contrasts, normalized with the maximum contrast obtained with R1, to compare the three measures made in points P1–P3. In the right column, we show the reduced spatial contrast (i.e., using the reduced grid shown in Fig. 1) for point P4 when recording the forward phase in the R1 configuration and the backward phase in a random configuration at a given distance from R1.

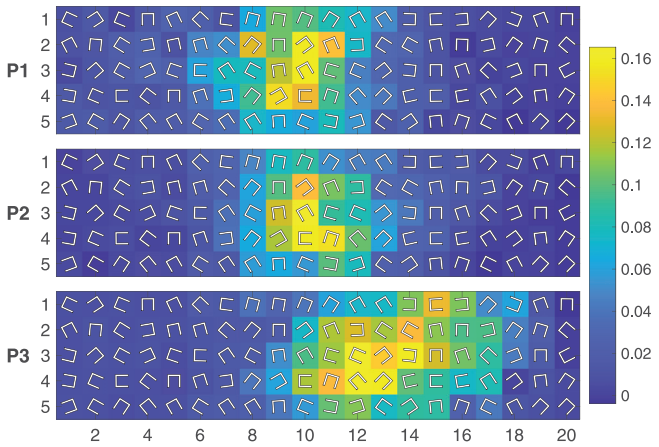

FIG. 7. (Color online) The relative contrast for a rotation of 15 deg of each scatterer independently. This figure represents how sensitive the temporal contrast is to rotations of a single scatterer (i.e., moving the configuration in a single direction in the 100-dimensional space defined in Sec. II G) by means of the relative contrast perturbation magnitude. Each panel corresponds to a measuring point (P1–P3 in Fig. 1). This magnitude is defined as $1 - \mathrm{TC}_{\mathrm{rms}}^{\mathrm{pert}}/\mathrm{TC}_{\mathrm{rms}}$, where $\mathrm{TC}_{\mathrm{rms}}^{\mathrm{pert}}$ ($\mathrm{TC}_{\mathrm{RMS}}$) is the RMS temporal contrast measure of the perturbed (unperturbed) configuration.

lower than those in the unperturbed case, leading to positive values of the relative perturbation measure. As expected, not all scatterers have the same influence on the relative contrast variations, and the most influential are those close to the $x = 0$ axis (between columns 10 and 11), where the source is located. Also, there is a noticeable difference for the P3 measure point, located toward the lower right corner in the experimental setup diagram [the orientation of the sonic crystal in Fig. 7 is the same as that displayed in Fig. 1(a)]. In this last case, the more influential columns are also the columns located over a line joining the source and receiver.

V. DISCUSSION

In this work, we achieved a single-channel TR process with high spatial and temporal contrasts using a periodic composite material (a sonic crystal), a result which could seem in apparent contradiction with previous results (Derode *et al.*, 2001a; Tourin *et al.*, 2006). In fact, disorder has been posed as an essential requirement to achieve a high degree of spectral and spatial decorrelation, allowing a higher number of independent "grains" of information in the frequency bandwidth and a higher aperture for the TR process and, consequently, high temporal and spatial contrasts (Derode *et al.*, 2000). The periodic structure of the sonic (or phononic) crystals clearly decreases the degree of spatial decorrelation of the acoustic field compared to the case of a disordered medium, explaining the absence of spatial focusing that was reported by Tourin *et al.* (2006). However, it is not so clear if the spectral decorrelation is flawed in the same way as the spatial decorrelation. In fact, Tourin *et al.* (2006) found that the time compression (or temporal contrast) was higher when using a phononic crystal for frequencies within the first bandgap compared to a disordered medium.

Still, the question remains as to how we can obtain both high values of spatial and temporal contrasts using a periodic structure. It is worth noticing that our setup presents a fundamental difference compared to that of Tourin *et al.* (2006), it is composed of non-convex scatterers with much less symmetry than a cylinder. A consequence of this lack of symmetry can be seen in the band diagram [Fig. 1(c)], where it is apparent that the band structure of our sonic crystal is more entangled than the band structure of one made with cylinders (see, for example, for a similar system, Romero-García *et al.*, 2013) even for the case of the C0 configuration, and in the studied frequency range, it is densely populated with partial band gaps and negative refraction frequency bands, yielding multiple posible wave vectors for a given temporal frequency. This can contribute to the spectral decorrelation of the signal because we are using an extremely large bandwidth compared to the one used by Tourin *et al.* (2006). Also, the random contribution made by the rotations of the columns could eventually be responsible for the spatial decorrelation of the acoustic field, which is similar to that obtained using a completely disordered medium, especially for higher frequencies.

To quantify this, we performed a complementary study on the spatial correlation of the impulse responses obtained for an ordered (C0) and random (R1) configuration as a function of the frequency.

We computed the TR operator, as defined in Eq. (12), integrating the TR transfer function over the full frequency range (0.5–20 kHz), and restricting the integration domain to three frequency bands: (a) low (0.5–1 kHz), (b) medium (1–4 kHz), and (c) high (4–20 kHz). The results for the ordered (TR^{C0}) and random (TR^{R1}) configurations are displayed in Fig. 8. These are $M \times M$ matrices where, as we mentioned in Sec. II F, each row can be interpreted as the normalized acoustic field at the time of reversal for all measurement points, and this replicates for each column corresponding to a different time-reversed impulse response. Therefore, a perfect TR would correspond to an identity matrix, and higher off diagonal values would correspond to a higher spatial correlation of the acoustic field and lower spatial contrast.

As the rectangular grid of measurement points are row-major ordered in the indices of these matrices, the points that are symmetric with respect to the $x = 0$ axis (as in the experimental setup) are located in 13 segments of 25 elements each perpendicular to the main diagonal at the $x = 0$ measurement points. These segments are visible in the TR^{C0} matrix of the ordered configuration for the wideband case (light red lines in Fig. 8, upper panel, first column) indicating that a positive correlation is always observed. This is due to the fact that for the ordered configuration, the symmetry of the experimental setup is perfect. Therefore, each time that a pulse is reversed at the location (x,y), a secondary pulse of equal magnitude is formed at the location $(-x, y)$. This symmetry is broken for the disordered configuration (R1), a slight anti-correlation is observed (light blue lines parallel to the main diagonal in Fig. 8, lower panel, first column) at the two neighboring

https://doi.org/10.1121/10.0005196

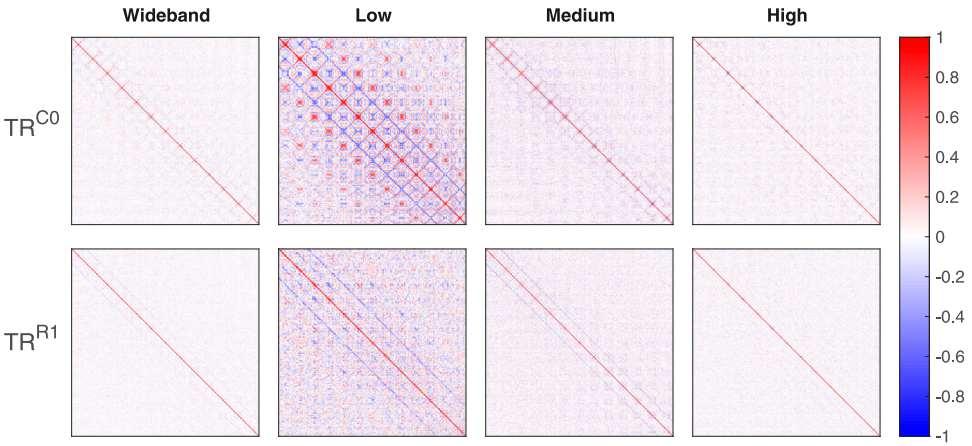

FIG. 8. (Color online) The TR matrices defined by Eq. (12) are integrated over the full (0.5–20 kHz, wideband), low (0.5–1 kHz), medium (1–4 kHz), and high (4–20 kHz) frequency ranges. Each *j*th column of the matrices corresponds to the amplitude values of the acoustic field at the 325 measurement points at the time of reversal when the reversed *j*th impulse was used as a signal in the second stage of the TR process.

points along the *y* axis. This sets a reasonable upper bound to the correlation length of the field, which is about the length of the grid spacing (15 cm).

The lower degree of spatial correlation for the disordered configuration compared to the ordered one is also observed in the low-, medium-, and high-frequency bands (Fig. 8). A dramatic example of the long-range correlations can be noticed in the TR matrix of the ordered configuration for the case of the low-frequency band, whereas the matrices for the random configuration display only local correlations from around three neighboring measurement sites for the low-frequency band to an almost perfect main diagonal (a correlation length less than the distance between the measurement points) for the higher frequencies. This last observation is consistent with the hypothesis that the random angles of the columns in the R1 configuration break the spatial correlation induced by the periodic structure of the sonic crystal (particularly for medium and high frequencies) because the correlations of the field are local and mainly produced by the length of the shortest wavelength.

The previous analysis could explain why the random configuration of the sonic crystal behaves as a multiple scattering medium with the needed degree of spatial and spectral decorrelation to achieve a TR process with high spatial and temporal contrasts. However, this does not clarify how this system compares to a truly disordered medium. To address this issue, we will compare the impulse responses generated by our system with a shot noise model that is widely used in the literature to simulate the response of an ideal heterogeneous medium.

The shot noise model is obtained as a superposition of pulses that follows a Poisson point process in time. This model can describe the ideal impulse response of a high-order disordered scattering medium where each pulse corresponds to a different multiple-scattering path (Haworth *et al.*, 2009). We also incorporate three additional features that extend this model so that it applies to our particular system without losing its intrinsic random nature. The first feature is a random phase applied to each pulse bandwidth-limited between 0.5 and 20 kHz. The second feature corresponds to a convolution of the model with the actual electroacoustic response of the audio system used in the experiment (real pulse). The last feature is a temporal decay that matches the average temporal decay of the impulse responses obtained in the measuring region. It is worth noting that this temporal decay is mainly due to the expansion of the propagating wavefront and it is observed even for frequencies where the acoustical energy absorption is negligible.

For these models, as a measure of the degree of spatial correlation, we calculated the RMS values of the off diagonal elements of the matrix TR given by Eq. (12). The results are displayed in Table I.

It is worth noticing that the addition of the real loudspeaker anechoic impulse response already introduces a lower limit to the correlation. This is consistent with the observation made by Derode *et al.* (2000) that for an ideal heterogeneous medium, the temporal and spatial correlations are those of the original pulse. The most striking result is that adding a temporal decay comparable to the decay of the measured impulse response is enough to fill the gap between the correlation value of our system and that of an ideal shot noise model.

To explain this result, we will put aside the RMS calculation and concentrate on two arbitrary measurement points x_1 and x_2 with random impulses responses $h_1^0(t)$ and $h_2^0(t)$ generated by the shot noise model. In the frequency domain, the time-reversed pulse at the point $\boldsymbol{x}_1$ corresponds to the evaluation of $H_1^0(\omega)^T H_1^0(\omega)$, where $H_1^0(\omega)$ is the transfer function at that point. Likewise, the response in x_2 for the same TR process corresponds to evaluating $H_1^0(\omega)^T H_2^0(\omega)$. The key point is that the integral over the frequency domain can be interpreted in two ways: (a) as the spatial correlation

TABLE I. The spatial correlation measured as the RMS values of the off diagonal elements of the TR matrices [Eq. (12)] for the shot noise models and sonic crystal scattering media.

Model	Ideal pulse	Real pulse
Shot noise	0.000265	0.000783
Shot noise random Phase	0.000265	0.000741
Shot noise/Temporal Decay	0.0013	0.0014
Sonic crystal/random configuration	—	0.0016
Sonic crystal/ordered configuration	—	0.0019

of the acoustic field between the points x_1 and x_2 [this is the interpretation of the previous analysis and of Eq. (12)], and (b) as the inverse Fourier transform of this product at the time of reversal (when $t=0$, $e^{i\omega t}=1$). This inverse Fourier transform is the cross correlation between $h_1^0(t)$ and $h_2^0(t)$ evaluated at $t=0$. Therefore, to compute the spatial correlation of the shot noise between x_1 and x_2, we must evaluate the expectation value of the cross correlation of their impulse responses at the time of reversal. Even when the impulse responses of x_1 and x_2 are completely uncorrelated, the introduction of the decay time leads to more energy in the beginning of the impulse and raises the expectation value of the cross correlation at the time of reversal. This observation is consistent with Haworth *et al.* (2009), who derived a statistical approximation for the expectation value of the TR focused signal in the case of the shot noise model with a temporal decay showing an increase along with the time constant of the decay.

The temporal decay introduces a characteristic time and, consequently, a slope in the cross correlation function. This raises the value of this function at $t=0$, which, as we have shown before, is equivalent to the spatial correlation between the two points. This analysis proposes that the differences between the scattered field of the sonic crystal in the random configuration and that of an ideally heterogeneous scattering medium may be mainly due to the temporal decay of the impulse response. As a consequence, our system, even endowed with a periodic structure, is capable of refocusing a time-reversed pulse with spatial and temporal contrasts comparable to those of an ideal inhomogeneous scattering medium.

VI. CONCLUSIONS

In this paper, a single-channel TR process of acoustical waves in the audible range with high temporal and spatial contrasts is obtained using a tunable sonic crystal as a medium. Previous works highlighted the importance of multiple and decorrelated wavefronts arriving at the receptor during the first stage of the TR process to achieve high contrast values. Sonic crystals have features that favour (multiple scattering units) and hinder (periodic structure) this decorrelated wavefront condition. The tunable sonic crystal presented here is endowed with two additional features that may further contribute to the number and decorrelation of the transmitted wavefronts and are proposed as an explanation for the successful TR process. The first feature is the convex shape of the scatterers, which induces a more entangled band diagram (compared to a scatterer with the same symmetry as the lattice), increasing the number of modes of propagation. The second feature is the random orientation of the scatterers, which breaks the translation symmetry of the lattice and decorrelates the arriving signal at the recording point.

It was also shown that the spatial decorrelation of the sonic crystal using a random orientation of the scatterers is comparable to that obtained using a shot noise model with an exponential time decay adjusted to the wideband experimental data. In this way, the tunable sonic crystal is able to time reverse an initial acoustic pulse as for other previously studied complex media (Derode *et al.*, 1995; Derode *et al.*, 2003). The novelty of the system under study is that this TR process can be turned on and off by changing the orientation of the columns, and this is mechanically accomplished using a simple motor system in a few seconds. Indeed, the time-reversed pulse obtained using the impulse response of a particular configuration is preserved only for configurations that are a few degrees apart from the original configuration and is lost for all the other possible configurations. This ability to switch on and off the time-reversed pulse can be exploited for applications in acoustical communication systems using physical encryption.

ACKNOWLEDGMENTS

The authors have received funding from Consejo Nacional de Investigaciones Científícas y Técnicas (CONICET) Grant No. PIP-11220130100573CO and Universidad Nacional de Quilmes Grant No. 827–1308/19.

[1]See supplementary material at https://www.scitation.org/doi/suppl/10.1121/10.0005196 for complementary figures S1–S7.

Alberti, A., Wisniacki, D. A., Maffei, G., and Eguia, M. C. (**2019**). "Effect of chaos in a one-channel time-reversal acoustic mirror," Phys. Rev. E **100**(1), 012208.

Anderson, B. E., Pieczonka, L., Remillieux, M. C., Ulrich, T. J., and Le Bas, P.-Y. (**2017**). "Stress corrosion crack depth investigation using the time reversed elastic nonlinearity diagnostic," J. Acoust. Soc. Am. **141**(1), EL76–EL81.

Blomgren, P., Papanicolaou, G., and Zhao, H. (**2002**). "Super-resolution in time-reversal acoustics," J. Acoust. Soc. Am. **111**(1), 230–248.

Cassereau, D., and Fink, M. (**1993**). "Focusing with plane time-reversal mirrors: An efficient alternative to closed cavities," J. Acoust. Soc. Am. **94**(4), 2373–2386.

Cervera, F., Sanchis, L., Sanchez-Perez, J. V., Martinez-Sala, R., Rubio, C., Meseguer, F., Lopez, C., Caballero, D., and Sanchez-Dehesa, J. (**2001**). "Refractive acoustic devices for airborne sound," Phys. Rev. Lett. **88**(2), 0239021–0239024.

Derode, A., Roux, P., and Fink, M. (**1995**). "Robust acoustic time reversal with high-order multiple scattering," Phys. Rev. Lett. **75**(23), 4206–4209.

Derode, A., Tourin, A., de Rosny, J., Tanter, M., Yon, S., and Fink, M. (**2003**). "Taking advantage of multiple scattering to communicate with time-reversal antennas," Phys. Rev. Lett. **90**(1), 014301.

Derode, A., Tourin, A., and Fink, M. (**1998**). "Time reversal in multiply scattering media," Ultrasonics **36**(1-5), 443–447.

Derode, A., Tourin, A., and Fink, M. (**2000**). "Limits of time-reversal focusing through multiple scattering: Long-range correlation," J. Acoust. Soc. Am. **107**(6), 2987–2998.

Derode, A., Tourin, A., and Fink, M. (**2001a**). "Random multiple scattering of ultrasound. I. Coherent and ballistic waves," Phys. Rev. E **64**(3), 036605.

Derode, A., Tourin, A., and Fink, M. (**2001b**). "Random multiple scattering of ultrasound. II. Is time reversal a self-averaging process?," Phys. Rev. E **64**(3), 036606.

Farina, A. (**2000**). "Simultaneous measurement of impulse response and distortion with a swept-sine technique," 108th AES Convention, Paris, France, Preprint 5093, pp. 1–24.

Fink, M. (**2006**). "Time-reversal acoustics in complex environments," Geophysics **71**(4), SI151–SI164.

Fink, M., Cassereau, D., Derode, A., Prada, C., Roux, P., Tanter, M., Thomas, J.-L., and Wu, F. (**2000**). "Time-reversed acoustics," Rep. Prog. Phys. **63**(12), 1933–1994.

Fink, M., Montaldo, G., and Tanter, M. (**2003**). "Time-reversal acoustics in biomedical engineering," Annu. Rev. Biomed. Eng. **5**, 465–497.
Haworth, K. J., Fowlkes, J. B., Carson, P. L., and Kripfgans, O. D. (**2009**). "Generalized shot noise model for time-reversal in multiple-scattering media allowing for arbitrary inputs and windowing," J. Acoust. Soc. Am. **125**(5), 3129–3140.
Hudin, C., Lozada, J., and Hayward, V. (**2014**). "Spatial, temporal, and thermal contributions to focusing contrast by time reversal in a cavity," J. Sound Vib. **333**(6), 1818–1832.
Kaina, N., Lemoult, F., Fink, M., and Lerosey, G. (**2015**). "Negative refractive index and acoustic superlens from multiple scattering in single negative metamaterials," Nature **525**(7567), 77–81.
Lemoult, F., Fink, M., and Lerosey, G. (**2011**). "Acoustic resonators for far-field control of sound on a subwavelength scale," Phys. Rev. Lett. **107**(6), 064301.
Lemoult, F., Kaina, N., Fink, M., and Lerosey, G. (**2013**). "Wave propagation control at the deep subwavelength scale in metamaterials," Nat. Phys. **9**(1), 55–60.
Lu, M.-H., Zhang, C., Feng, L., Zhao, J., Chen, Y.-F., Mao, Y.-W., Zi, J., Zhu, Y.-Y., Zhu, S.-N., and Ming, N.-B. (**2007**). "Negative birefraction of acoustic waves in a sonic crystal," Nat. Mater. **6**(10), 744–748.
Ma, F., Chen, J., and Wu, J. H. (**2020**). "Time-delayed acoustic sink for extreme sub-wavelength focusing," Mech. Syst. Signal Process. **141**, 106492.
Ma, G., Fan, X., Ma, F., De Rosny, J., Sheng, P., and Fink, M. (**2018**). "Towards anti-causal Green's function for three-dimensional sub-diffraction focusing," Nat. Phys. **14**(6), 608–612.
Montaldo, G., Lerosey, G., Derode, A., Tourin, A., de Rosny, J., and Fink, M. (**2004**). "Telecommunication in a disordered environment with iterative time reversal," Waves Random Media **14**(3), 287–302.
Papanicolaou, G., Solna, K., and Ryzhik, L. (**2004**). "Statistical stability in time reversal," SIAM J. Appl. Math. **64**(4), 1133–1155.
Ribay, G., de Rosny, J., and Fink, M. (**2005**). "Time reversal of noise sources in a reverberation room," J. Acoust. Soc. Am. **117**(5), 2866–2872.
Romero-García, V., Lagarrigue, C., Groby, J., Richoux, O., and Tournat, V. (**2013**). "Tunable acoustic waveguides in periodic arrays made of rigid square-rod scatterers: Theory and experimental realization," J. Phys. D: Appl. Phys. **46**(30), 305108.
Sanchez-Perez, J. V., Caballero, D., Martinez-Sala, R., Rubio, C., Sanchez-Dehesa, J., Meseguer, F., Llinares, J., and Gálvez, F. (**1998**). "Sound attenuation by a two-dimensional array of rigid cylinders," Phys. Rev. Lett. **80**(24), 5325–5328.
Shimura, T., Ochi, H., and Song, H. C. (**2013**). "Experimental demonstration of multiuser communication in deep water using time reversal," J. Acoust. Soc. Am. **134**(4), 3223–3229.
Tourin, A., Van Der Biest, F., and Fink, M. (**2006**). "Time reversal of ultrasound through a phononic crystal," Phys. Rev. Lett. **96**(10), 104301.
Vigo, D. G. A., Fouque, J.-P., Garnier, J., and Nachbin, A. (**2004**). "Robustness of time reversal for waves in time-dependent random media," Stochast. Process. Appl. **113**(2), 289–313.
Yon, S., Tanter, M., and Fink, M. (**2003**). "Sound focusing in rooms: The time-reversal approach," J. Acoust. Soc. Am. **113**(3), 1533–1543.